Volcanic Process Ground Deformation Using DInSAR Observations: The Case Study of the Sabancaya Volcano

Micaela Castellani [1], Sebastian Balbarani [2] and Mauricio Gende [1,3]

[1] Facultad de Ciencias Astronómicas y Geofísicas, Univ. Nacional de La Plata. Argentina - (micacflores, mgende)@fcaglp.unlp.edu.ar
[2] Depto. Agrimensura, FI-UBA y Lab. Geociencias, FIE-UNDEF. Argentina - (sbalbara@fiu.uba.ar)
[3] Consejo Nacional de Investigaciones Científicas y Técnicas-CONICET. Argentina

Keywords: Surface deformation, DInSAR, Sentinel-1, Volcanology, Sabancaya

Abstract

Remote sensing is one of the most useful tools when it comes to studying earth phenomena along large terrain extensions. Within this broad field, Differential Interferometric Synthetic Aperture Radar (DInSAR) has been evolving, and at this point is able to provide terrain deformation in millimetre-level precision. This analysis was conducted over the Sabancaya Volcano, in Perú, which is part of the Ampato-Sabancaya Volcanic Complex. This volcano has been active and continuously erupting since 2016, with various fault systems surrounding the volcanic complex. The main objective of this work was to map deformation caused by the volcanic system, processing Sentinel-1 products from 2016 and an interval that started in 2014 to 2017 to be able to study the effects of temporal decorrelation on interferometric products, being Sentinel-1 the first of the Copernicus Program satellite constellations conducted by the European Space Agency. The analysis showed deformation in the interval in which the eruption started and a deformation centre in the northern region of the volcanic complex, although the last one was found when studying a longer temporal baseline. Overall, the experiment shows that DInSAR is an effective tool to study volcanic systems.

1. Introduction

The analysis of deformation on the Earth's surface is essential for understanding geodynamic processes and predicting potentially catastrophic geological events. In the case of volcanic systems, studying their movements and changes is crucial for generating early eruption alerts, as well as for understanding and modelling them.

Volcanic monitoring is a multidisciplinary field, and among its various techniques is Differential Interferometric Synthetic Aperture Radar (DInSAR), which stands out for its ability to detect displacements over large areas with high precision and spatial resolution. DInSAR is a remote sensing technique that uses radar images captured by instruments mounted on satellites to measure millimetric changes on the Earth's surface over time, even in hard-to-reach areas and under any weather conditions (Hermosilla, 2016).

The DInSAR technique uses phase information from SAR products to obtain a measurement of displacement in the Line of Sight (LOS) direction, which is perpendicular and to the right of the flight direction. This displacement in LOS can then be divided indisplacement in the East-West and Up-Down direction (Hassen, 2001).

This work is focused around the Sabancaya volcano, which is the second most active volcano of the Southern Perú volcanic arc. It has been active and emitting volcanic material nonstop since 2016, although seismic-volcanic activity began around 2014 (IGP, 2023). Sabancaya is a stratovolcano part of theAmpato-Sabancaya Volcanic Complex (71° 49'–71° 54' W; 15° 46'–15° 52' S), along with two other inactive volcanos, Hualca- Hualca and Ampato. It is important to mention that there are a number of small towns close to the Volcanic Complex, which makes understanding the volcanic system a priority in order to beable to issue early alerts. Since the eruption started on November 6th, 2016, we usedSentinel-1 images in order to measure displacement in the area ofinterest.

The images were provided by the Sentinel-1 mission, which is the first of the Copernicus Program satellite constellations conducted by the European Space Agency (ESA).The selected images were taken before and after the start of the eruption. In addition, since temporal decorrelation is an important issue when it comes to interferometric products, an analysis from 2014 to 2017 was made.

2. Area of Interest and Geological Context

The origin of the Ampato-Sabancaya Volcanic Complex (CVASfrom now on) is a product of the Andes Mountain range, which began as a result of the subduction of the Nazca plate under the South American tectonic plate. The CVAS is geologically young,with the Hualca Hualca volcano being the first to form in the Pliocene. Later, the Ampato volcano formed at the southern endin the early Pleistocene, and finally, the volcanism that gave riseto Sabancaya occurred during the late Pleistocene and has continued into the Holocene (Samaniego et al., 2016).

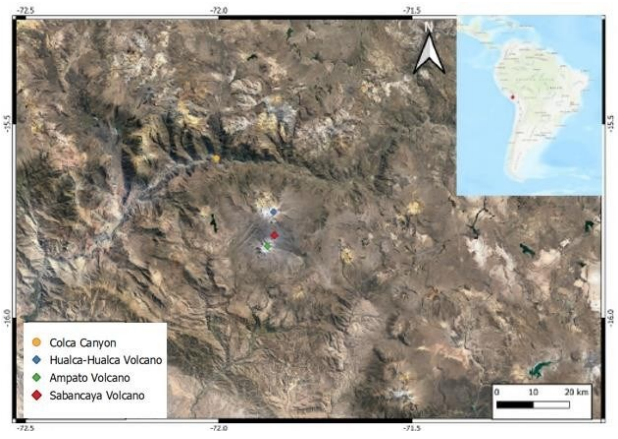

Figure 1. Location map of the Ampato-Sabancaya Volcanic Complex.

The Sabancaya volcano formed in three stages, with andesitic and dacitic lava flows and ash deposits. It has exhibited both effusive and explosive eruptive styles, including ash emissions, pyroclastic flows, and lava emissions. The study area has been defined as a 1500 km² zone that containsthe entire CVAS as well as the Colca Canyon (See Figure 1).

3. Methodology

For this analysis Sentinel-1 images were used, provided by the European Space Union (ESA) and available for download by the Alaska Satellite Facility (ASF) [1]

3.1 SAR Data

In this case, the SAR products used in the analysis were Interferometric Wide Swath (IW) Level-1 Single Look Complex (SLC), chosen in order to then make the displacement vector decomposition (See Figure 2). Each image is formed by three sub-swaths and nine bursts, covering a total area of 20000 km². Since the processing of an entire image has an impact on processing time, sub-swaths and bursts intervals were smaller and centred on the area of interest, where the Sabancaya volcano is located.

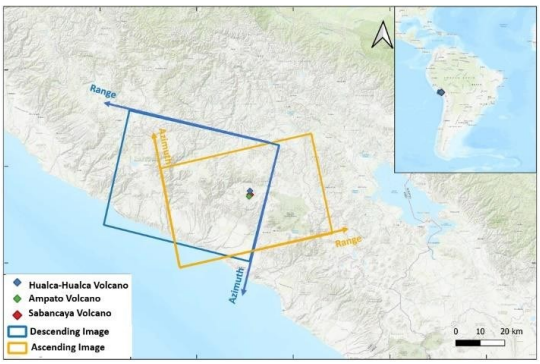

Figure 2. Sentinel-1 products above the CVAS

Since the eruption began on November 6th, 2016, images were selected before and after the event. Then, we decided to study a larger interval, from 2014 to 2017 in order to observe the impact of the temporal baseline in the case of this volcanic system. This analysis is based on the important characteristic of the Sentinel-1 mission, which has an orbital tube of +/- 120 m where the satellites are constrained, which makes the positioning of them more precise. This allows to take larger time intervals between images without loss of information, at the cost of increased noise. The images were selected having in mind three key aspects: they must cover the entire area of interest to avoid border effects, they have to have the same processing level SLC and the same Path to avoid any geometric errors due to satellite orbit change.
The images selected are listed in Table 1.

Reference	Date	Orbit	Path	Frame
A1	15/10/2016	Ascending	47	1125
A2	8/11/2016	Ascending	47	1125
D1	26/10/2016	Descending	25	643
D2	19/11/2016	Descending	25	643
A3	8/10/2014	Ascending	47	1125
A4	16/09/2017	Ascending	47	1125
D3	12/11/2014	Descending	25	641
D4	15/09/2017	Descending	25	641

Table 1. Images selected for analysis

3.2 DInSAR Processing

The image processing was carried out using the Sentinel Application Platform Software (ESA,2023). The processing starts with “splitting” the images to centre them around the area of study. Since the Interferometric Wide Swath has 3 sub swaths and 9 bursts, for all ascending images, IW1 was used for a 5 to 9 interval, while descending images were processed with a IW2 sub swath and a 5 to 9 burst interval. The precise Sentinel-1 orbit files were applied to all products.

To create the interferogram, a corregistration is applied to align the images at a sub-pixel level (Hassen, 2001). This meansthat there’s a reference image, or master, which is the image acquired before the event, and a slave image, which is acquired after. To align the images, the slave image is interpolated using a Digital Elevation Model to have the same pixels as the master image. The DEM used in this case was 90 m Shuttle Radar Topographic Mission (SRMT) provided by NASA because of its good coverage of the area of interest and its resolution.

The interferogram was formed for each pair of images (A1-A2, D1-D2, A3-A4 and D3-D4), and since they are SLC images, each of its pixels has a complex value that contains the information about the Amplitude and Phase. The interferogram consists in the crossed multiplication of the master image with the complex conjugate slave image (Calvet, 2022). Since each pixel contains a complex number, thisresults in multiplication of amplitude and phase subtraction. This last value is the one that holds important information about displacement, topographic and atmospheric delays, orbital errors, tropospheric errors and white noise (Richards, 2009). The products of the interferogram formation are real numbers which allow calculated bands of Intensity and Phase, and the Coherencevalue for each pixel. This last band is important when it comes toproduct interpretation.

In order to calculate the phase difference due to displacement, a topographic phase removal is applied, using the same DEM as before. Now, the interferogram is formed and can be filtered to get better results to analyse. Multilooking is a great tool to reduce random noise present in the interferogram, but it can reduce resolution, since it uses the same image as a filter. The Multilook is a grid in Range and Azimuth. For A1-A2 and D1-D2 a Multilook of 4x1 was applied, while for A3-A4 and D3-D4 a Multilook of 40x10 was applied because of its high speckle presence due to its longer temporal baseline.

When it comes to filtering, a Goldstein filter (Goldstein et al., 1998) was applied to all the interferograms to help with visual interpretation. Since this filter works in the Fourier domain, the Fast Fourier Transform window size is 64 and the filter window size is 5 by 5. With this filter the interferogram was formed, with a wrapped phase that goes from [-π, π]. But the continuous and unwrapped phase value is needed in order to find the displacement value by Equation 1 (Rosell, 2022).

$$\Delta\phi = -\frac{4\pi}{\lambda} d_{LOS} \quad (1)$$

where ϕ = phase
d_{LOS} = Displacement in LOS direction
λ = wavelength of Sentinel-1 mission (5.6 Hz)

We have $\Delta\phi$ and need to find d_{LOS}, but in order to achieve that, a continuous phase value is needed so a phase unwrapping algorithm is applied. There are several ones (Golstein et al., 1988; Hassen, 2001) but in this case we applied the SNAPHU algorithm (Chen et al., 2002) which uses the Minimal Cost Flow method

[1] https://search.asf.alaska.edu/#/

[2] https://www.earthdata.nasa.gov/sensors/srtm

(Goldstein et al., 1988). This method works by constructing a network flow model where the cost is minimized to determine the most consistent phase values across the image. Essentially, it finds the smoothest transition between phase values while minimizing errors, which helps in generating more accurate surface measurements.

After having the unwrapped phase, using Equation (1) and knowing that Sentinel-1 operates in the C Band, we could find the displacement in LOS direction. These values were in SAR coordinates, so we applied geocoding to convert from SAR to WGS84geographic coordinates. The displacement vector in LOS direction can be decomposed into displacement in the east-west and up-down directions (See Figure 3).

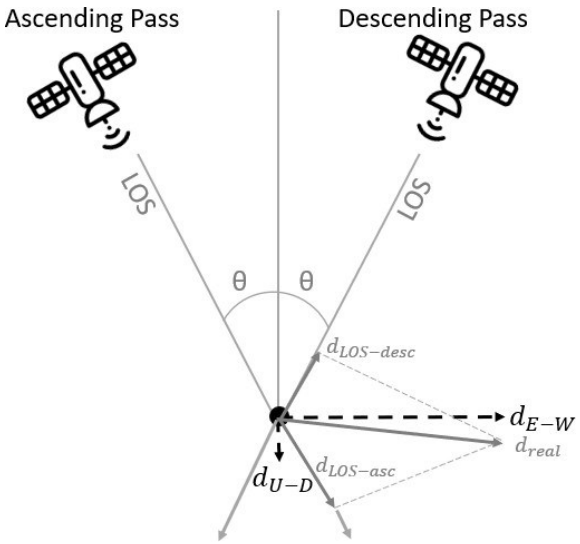

Figure 3. Displacement in LOS decomposed in Up-Down (U-D) and East-West (E-W) directions from the Ascending and Descending interferograms.

In this case, if we wanted to obtain the North-South component we should have more observations in order to find that variable. Since we have ascending and descending orbit, we assume N-S component is small in comparison to the other componentsand we will study E-W and Up-Down. This decomposition (Eq. 2 and Eq. 3) can be made by combining a descending and an ascending orbit, and assuming a constant incidence angle of θ = 36º and a geographic azimuth of approximately 90º for theascending orbit and 270º for the descending one (Hassen, 2001).

$$d_{LOS}^{asc} = d_{EW}\sin(\varphi_{asc})\sin(\theta) + d_{NS}\cos(\varphi_{asc})\sin(\theta) + d_{UP}\cos(\theta) \quad (2)$$

$$d_{LOS}^{des} = d_{EW}\sin(\varphi_{des})\sin(\theta) + d_{NS}\cos(\varphi_{des})\sin(\theta) + d_{UP}\cos(\theta) \quad (3)$$

Replacing with the aprroximate azimuth values, and solving the displacements in the E-W and Up-Down directions gives:

$$d_{EW} = \frac{d_{LOS}^{asc} - d_{LOS}^{des}}{2\sin(\theta)} \quad (4)$$

$$d_{EW} = \frac{d_{LOS}^{asc} + d_{LOS}^{des}}{2\cos(\theta)} \quad (5)$$

where φ_{asc} = Azimuth for the ascending orbit
φ_{des} = Azimuth for the descending orbit
θ = Incidence angle

4. Results

4.1 DInSAR Analysis 2016

4.1.1 Ascending Pass

In this first case (See Figure 4) we can see high coherence (> 0,7) along the entire area of study except in parts where the topography gets more complex, such as the Colca Canyon. It can also be seen a loss in coherence above the volcanos, which can be expected due to possible shadowing. On the other hand, whenit comes to LOS Displacement, a maximum value of 1,89 cm is found on the north of the Hualca-Hualca volcano, while in the Sabancaya volcano the deformation is approximately of 1 cm. Noise can be seen on the LOS Displacement in the area of the Colca Canyon. This comes from the unwrapping algorithms, in which the result can induce error because of the steep topography changes. This induced error tends to be local and not spread across the entire study area. The resolution for both ascending and descending passes is 20x20 m.

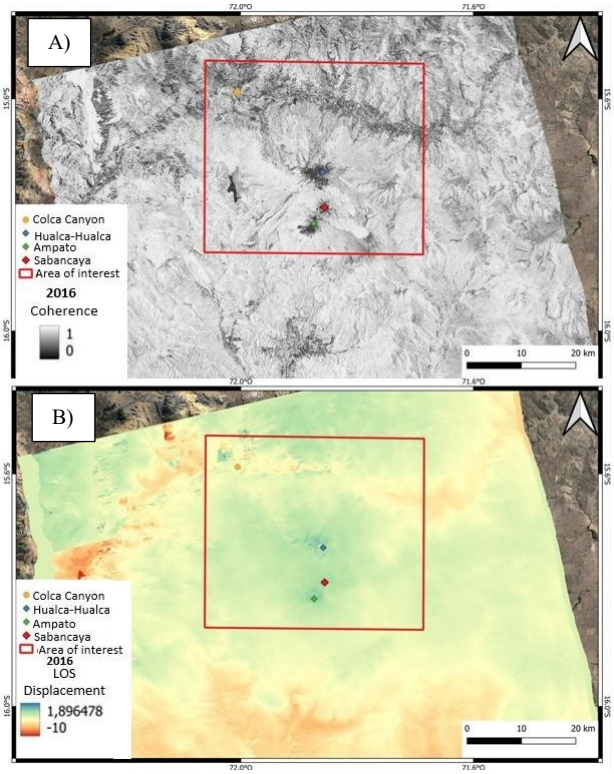

Figure 4. 2016 DInSAR products of coherence (A) and LOSDisplacement in cm (B) in the ascendent pass.

4.1.2 Descending Pass

For the descendent case (See Figure 5), the coherence is also high except in the parts with challenging topography. The LOS Displacement in this case is a little bit higher, with a maximum of 3.15 cm in the three volcanoes. This difference between the ascending and descending pass could be due to the difference with the angle in which the radiation strikes the Earth's surface.

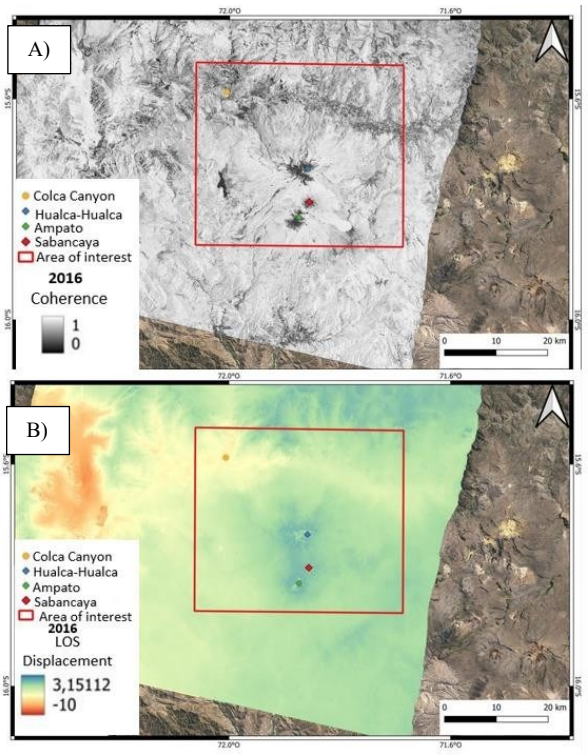

Figure 5. 2016 DInSAR products of coherence (A) and LOS Displacement in cm (B) in the descendent pass.

4.1.3 Displacement products

The vertical displacement seen in Figure 6 presents a maximum value of approximately 1.9 cm in the area where the volcanos are located, which can be interpreted as deformation due to the start of the Sabancaya eruption. While the vertical component shows these values, the horizontal E-W displacement shows very small values, close to zero. This means that the deformation process is associated with the inflation of the volcanic system.

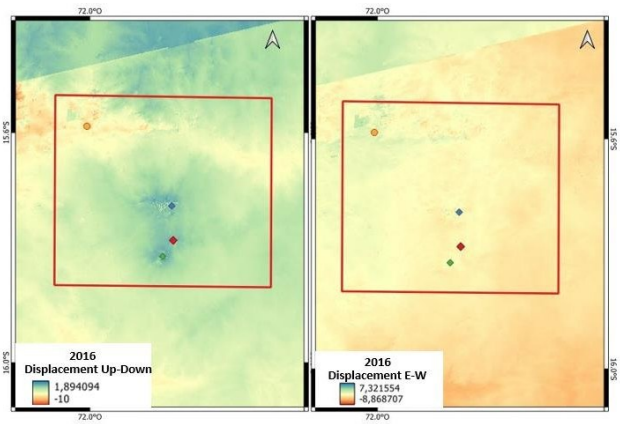

Figure 6. 2016 Vertical Displacement U-D (Left) and E-W (Right) in cm.

4.2 DInSAR Analysis 2014-2017

4.2.1 Ascending Pass

For the 2014-2017 case (See Figure 7) the coherence of the interferogram is low due to temporal decorrelation, since the temporal baseline for this case is 1074 days. Since the seasonin which the images have been taken is the same, decorrelationdue to seasonal changes is unlikely. A large cumulative deformation centre can be spotted on the north-west part of the CVAS, which may indicate that the volcanic material erupting from the Sabancaya volcano has its origin in a chamber located in the north part of the CVAS. This result matches with the work from Boixart et al. in 2020, that consisted in using DInSAR and GNSS to put together a source model for Sabancaya, and concluded that there may be a deep reservoir that continuously feeds the Sabancaya and that would explain the expulsion of material that started in 2016 and keeps going until the publication of this article, in 2024.

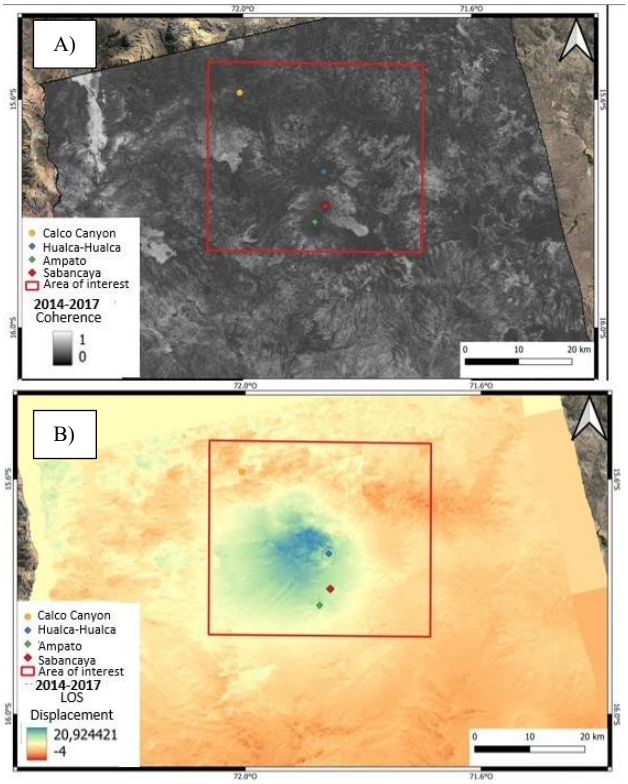

Figure 7. 2014-2017 DInSAR products of coherence (A) and LOSDisplacement in cm (B) in the ascending pass.

4.2.2 Descending Pass

The coherence observed in Figure 8 is low as seen in the ascending product. In both of them, emerging from the Sabancaya can be seen a lava flow that has higher coherence. The stable, unchanging nature of the cooled lava allows the radar signals to maintain phase consistency between acquisitions, leading to higher coherence. This phenomenon is also evident in the ascending pass, reinforcing the idea that solidified volcanic material plays a key role in maintaining coherence in interferometric radar data.

As for the LOS displacement, a maximum of almost 15 cm can be observed in the northern part of the CVAS, and again, the error induced by the unwrapping algorithm can be appreciated in the Colca Canyon area.

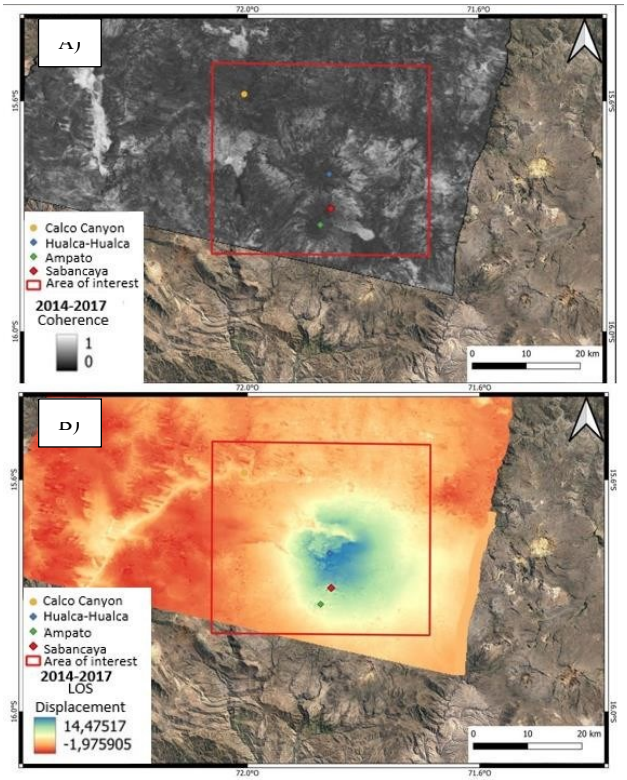

Figure 8. 2014-2017 DInSAR products of coherence (A) and LOS Displacement in cm (B) in the descending pass.

4.2.3 Displacement products

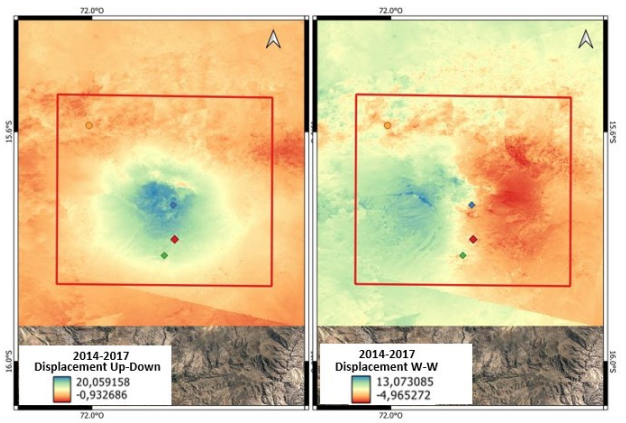

Figure 9. 2014-2017 Vertical Displacement U-D (Left) and E-W (Right) in cm

In the temporal interval of Figure 9, a cumulative displacement of 20 cm in the vertical displacement can be observed in the northern part of the CVAS and the ratio of deformation is almost 10 km.

As for the horizontal deformation, the area where the volcanoes are located is almost zero, while on the east side it tends to show negative values and on the west part it tends to show positive values. This result matches with GNSS observations found in the IGP Technical Report (IGP,2023), where very small horizontal movement was found in GNSS stations located near the volcanoes.

5. Discussion and Conclusion

Based on the results obtained, we may say that the Sabancaya volcano is not a violent eruptive system that generates large terrain changes. It is dynamic and has a continuous material emission which creates larger changes when comparing longer temporal baselines. On the other hand, comparing larger temporal intervals brings larger temporal decorrelation, which introduces more noise into the products.

The vertical deformation from the year 2016 showed maximum values of almost 2 cm, while the cumulative deformation in the interval 2014-2017 had a maximum of almost 20 cm. This larger deformation was located on the northern part of the CVAS, which would mean that there is a deep reservoir from which the Sabancaya gets its eruptive material. According to Boixart et al. (2020), this reservoir could be 10 to 12 km deep and it is located 5km north from the Sabancaya Volcano, which coincides with the centre of deformation found.

It is typically expected that volcanic areas experience inflation prior to an eruption, as magma accumulates beneath the surface, followed by deflation once the volcano begins releasing material, as seen in the case of Sabancaya. This inflation-deflation cycle is key to understanding the dynamics of volcanic activity. However, it is crucial to note that the deformation captured in this study represents cumulative movement over time. To achieve a more detailed analysis, the inclusion of additional satellite images would be necessary, allowing for the creation of a time series that tracks deformation patterns more precisely. Time series analysis, by capturing continuous changes over specific intervals, would provide valuable insights into the temporal evolution of deformation, helping to distinguish between short-term transient signals and long-term deformation trends. This time series approach was done by the Geophysical Institute of Perú and according to the Technical Report from 2023 (IGP,2023), an area of positive deformation was found using temporal DInSAR series and GNSS. This inflation area has a deformation velocity that varies from 35 mm/yr to 50 mm/yr and is located about 5 km north of Sabancaya.

References

Boixart, G., Cruz, L., Cruz, R., Eullades, L., Battaglia, M., 2020. Source model for Sabancaya volcano constrained by DInSAR and GNSS surface deformation observation. *Multidisciplinary Digital Publishing Institute.*

Calvet, A., 2022: *Interferometría diferencial sar para detectar deformación cortical por actividad sísmica.* Master's tesis: Universidad Nacional de La Plata.

Chen, C. W., Zebker, H. A., 2002. Phase unwrapping for large SAR interferograms: statistical segmentation and generalized network models. *IEEE Trans. Geosci. Remote Sens. 40, 1709-1719.*

European Space Agency, 2023. *Sentinel Application Platform (SNAP) (Version 9.0)* [Software]. European Space Agency. https://step.esa.int/main/download/snap-download/

Goldstein, R. M., Wegner, C. L., 1998. Radar interferogram filtering for geophysical applications. *Geophysical Research Letters. 25, 4035-4038.*

Goldstein, R. M., Zebker, H. A. and Werner C. L., 1988. Satellite radar interferometry: Two-dimensional phase unwrapping. *Radio Science. 23, 713-720.*

Gomez Martin, 2021: *Interferometría de imágenes radar de apertura sintética aplicada a la deformación superficial del terreno: región de Bío Bío, Chile.* Master's tesis: Universidad de Salamanca.

Hassen, R. F., 2001: *Radar Interferometry*. Kluger Academic Publishers.

Hermosilla, E.D., 2016: *Interferometría de Radar de Apertura Sintética (InSAR) aplicada al estudio del movimiento de ladera aledaña al volcán Calcuco con ayuda de imágenes Sentinel-1A.* Master’s tesis: Universidad Técnica federico Santa María.

Instituto Geofísico del Perú (IGP), 2023: *Deformación en el entorno del volcán sabancaya y caraterización de la fuente a partir del modelado con datos gnss y dinsar del período 2014-2021*. Informe Técnico Nº 016-2023.

Richards, J. A., 2009. *Remote sensing with imaging radar*, Vol. 1, pp. 172-173. Berlin/Heidelberg, Germany: Springer.

Samaniego, P., Rivera, M., Mariño, J., Guillou, H., Liorzou C., Zerathe, S., Delgado, R., Valderrama, P., Scao, V., 2016. The eruptive chronology of the Ampato-Sabancaya volcanic complex (Southern Peru). *Journal of Volcanology and Geothermal Research. 32, 110-128.*

Rosell, P., 2022. *Desarrollo de un modelo de corrección de la influencia del vapor de agua troposférico en el procesamiento DInSAR con el aporte de GNSS y ERA5.* Universidad Nacional de Cuyo.